

ARTICLE OPEN



Reducing functionally defective old HSCs alleviates aging-related phenotypes in old recipient mice

Yuting Wang^{1,2,3}, Wenhao Zhang^{1,2,3}, Chao Zhang^{1,2,3} , Hoang Q. Tran Van^{1,2,3}, Takashi Seino^{1,2,3} and Yi Zhang^{1,2,3,4,5}

© The Author(s) under exclusive licence to Center for Excellence in Molecular Cell Science, Chinese Academy of Sciences 2024

Aging is a process accompanied by functional decline in tissues and organs with great social and medical consequences. Developing effective anti-aging strategies is of great significance. In this study, we demonstrated that transplantation of young hematopoietic stem cells (HSCs) into old mice can mitigate aging phenotypes, underscoring the crucial role of HSCs in the aging process. Through comprehensive molecular and functional analyses, we identified a subset of HSCs in aged mice that exhibit “younger” molecular profiles and functions, marked by low levels of CD150 expression. Mechanistically, CD150^{low} HSCs from old mice but not their CD150^{high} counterparts can effectively differentiate into downstream lineage cells. Notably, transplantation of old CD150^{low} HSCs attenuates aging phenotypes and prolongs lifespan of elderly mice compared to those transplanted with unselected or CD150^{high} HSCs. Importantly, reducing the dysfunctional CD150^{high} HSCs can alleviate aging phenotypes in old recipient mice. Thus, our study demonstrates the presence of “younger” HSCs in old mice, and that aging-associated functional decline can be mitigated by reducing dysfunctional HSCs.

Cell Research (2025) 35:45–58; <https://doi.org/10.1038/s41422-024-01057-5>

INTRODUCTION

The aging process is marked by a functional decline across various tissues and organs,^{1–3} which significantly increases the risk for a multitude of chronic diseases.⁴ Previous studies have shown that transfusion of young blood or its components into aged mice can have a rejuvenation effect,^{5–10} supporting an important role of the hematopoietic system in whole body aging. Hematopoietic stem cells (HSCs), the source of all hematopoietic cell types, undergo profound functional changes with age, including increased prevalence of clonal hematopoiesis, a shift toward myeloid-biased differentiation, and a diminished capacity for blood regeneration.^{11–15} Recent studies have shown that replacing HSCs of old mice with those of young mice can improve health and extend lifespan of old recipient mice.^{16–18} Conversely, transplanting aged HSCs into young mice can accelerate immune system aging and reduce their lifespan.^{19,20} These studies suggest that HSCs could serve as promising targets for aging-related intervention.

Previous studies have established that intrinsic alterations of HSCs with aging are associated with their functional decline, including increased DNA damage, mitochondrial degeneration, diminished asymmetric distribution of CDC42, altered H4K16 acetylation during mitosis, and other epigenetic modifications.^{21–27} Interestingly, the HSC population exhibits intrinsic heterogeneity in both young and old mice, distinguishable by lymphoid-biased, balanced, and myeloid-biased subtypes based on surface markers and lineage predispositions.^{28–36} Notably, a fraction of HSCs can preserve long-term dormancy and functionality during aging.^{37–39} However, the changes of HSC heterogeneity during aging and their contribution to systemic aging remain to be comprehensively characterized.

In this study, we demonstrate that transplantation of young HSCs can alleviate aging phenotypes in old mice. Single-cell sequencing (scrRNA-seq) reveals an increased aging heterogeneity in old HSCs. Systematic molecular and functional characterization indicate the presence of “younger” and functionally defective “older” subsets of HSCs in old mice, marked by differential expression levels of CD150. Mechanistically, old CD150^{high} HSCs exhibit differentiation defects compared to those of the CD150^{low} HSCs. Notably, transplantation of the “younger” subset of HSCs into old recipient mice can attenuate aging phenotypes, including decreased epigenetic age and extended lifespan of old recipient mice compared with those that received old un-selected HSCs or CD150^{high} HSCs. Importantly, reducing the dysfunctional CD150^{high} HSCs can attenuate aging phenotypes in old recipient mice, highlighting that the removal of defective CD150^{high} HSCs from old mice could be a potential strategy for rejuvenation.

RESULTS

Transplantation of young HSCs alleviates aging phenotypes in old recipient mice

To directly evaluate the functional differences between young and old HSCs in vivo, we sorted long-term (LT)-HSCs (lineage[−] c-Kit⁺ Sca-1⁺ (LSK) CD48[−] CD34[−] CD150⁺) (referred to as HSCs) from young and old mice (Supplementary information, Fig. S1a). Consistent with previous reports,^{12,13,40} a significant increase in the number of HSCs in old mice was observed (Supplementary information, Fig. S1b). Serial transplantation of both young and old HSCs into lethally irradiated young recipient mice (Fig. 1a) revealed a notable decline in the repopulation

¹Howard Hughes Medical Institute, Boston Children’s Hospital, Boston, MA, USA. ²Program in Cellular and Molecular Medicine, Boston Children’s Hospital, Boston, MA, USA.

³Division of Hematology/Oncology, Department of Pediatrics, Boston Children’s Hospital, Boston, MA, USA. ⁴Department of Genetics, Harvard Medical School, Boston, MA, USA.

⁵Harvard Stem Cell Institute, Boston, MA, USA. email: yzhang@genetics.med.harvard.edu

Received: 13 June 2024 Accepted: 8 November 2024

Published online: 2 January 2025

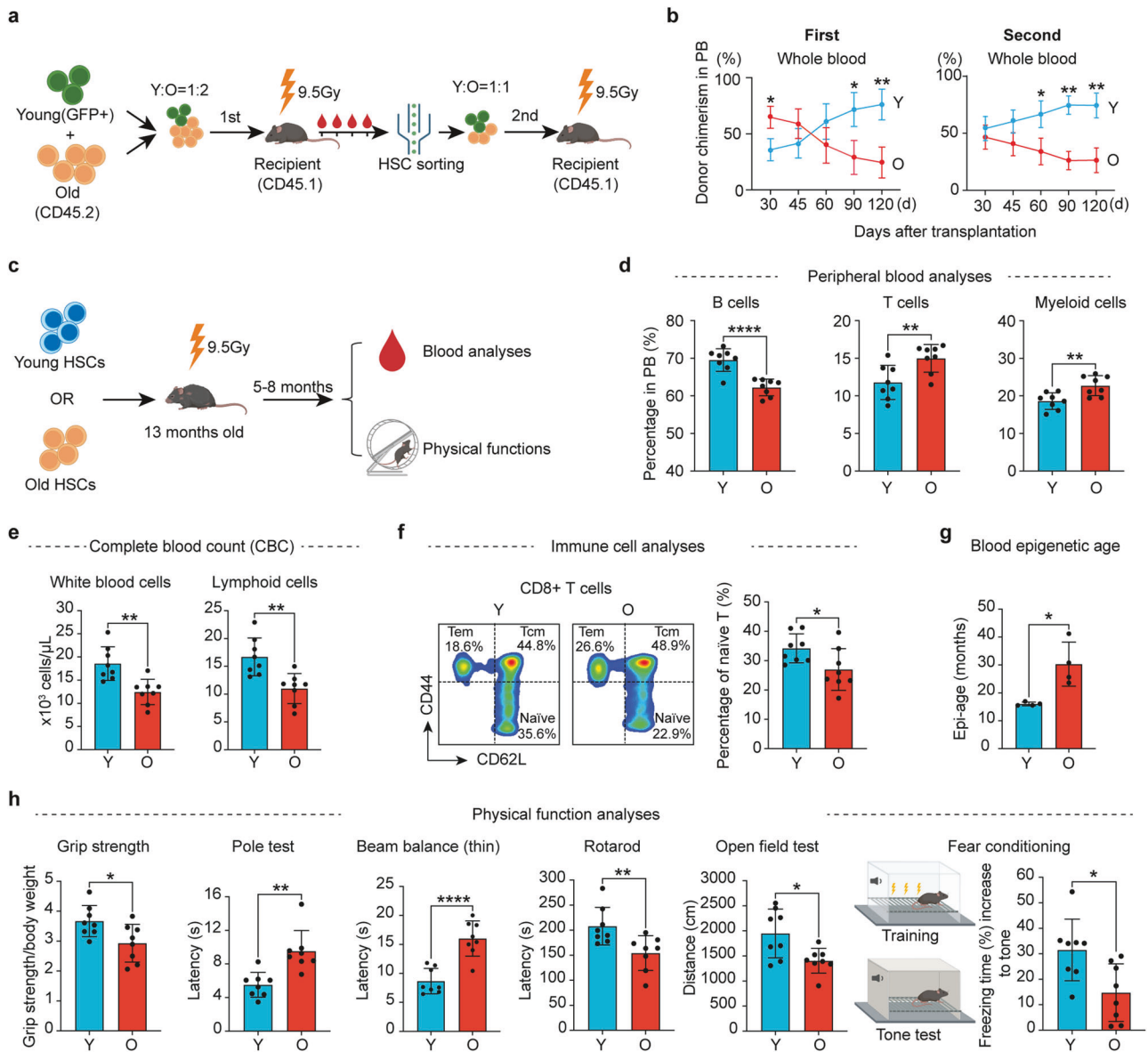


Fig. 1 Transplantation of young HSCs alleviates aging phenotypes in old recipient mice. **a** Diagram illustration of the competitive young (2–3 months) and old (22–24 months) HSC transplantation experiment. For the first transplantation, the ratio of young to old HSCs was 1:2 (500 young and 1000 old) while the ratio was 1:1 (1000 young and 1000 old) for the second transplantation. **b** Peripheral blood (PB) chimerism of donor HSCs at different time points after the 1st and 2nd transplantation, $n = 6$ for the first and $n = 3$ for the second transplantation. **c** Diagram showing the experimental design of individual transplantation of 1000 young (3 months) or 1000 old (22–24 months) HSCs into middle-aged recipients (13-month-old). Five months after the transplantation, a series of hematopoietic and physical tests were performed. **d** Bar graph showing the percentage of B, T and myeloid cells in the PB of recipient mice, $n = 8$. **e** Bar graph showing the absolute number of blood cells in the PB of recipient mice, $n = 8$. **f** FACS plot and bar plot showing the percentage of naïve T cells in CD8⁺ T cells from recipient mice, Naïve T cells (CD44^{low}, CD62L^{high}), Tcm (CD44^{high}, CD62L^{high}) and Tem (CD44^{high}, CD62L^{low}), $n = 8$. **g** Bar plot showing the epigenetic age of blood from recipient mice, $n = 4$. **h** Physical tests of recipient mice that received young or old HSCs. Muscle strength, motor coordination, endurance and brain function were assessed, $n = 8$. Mean \pm SD, Student's *t*-test, * $P < 0.05$, ** $P < 0.01$, **** $P < 0.0001$. The graphics of the mouse and equipment in **a**, **c** and **h** were created with BioRender.

capacity and biased differentiation of old HSCs compared to their young counterparts (Fig. 1b; Supplementary information, Fig. S1c–f). These results are consistent with previous studies,^{12,20} and confirm the age-related intrinsic decline of HSCs.

To analyze the contribution of HSCs to systemic aging, we transplanted young or old HSCs into irradiated middle-aged mice (13 months). Five months after transplantation, we evaluated the aging status of the recipient mice by performing blood analyses and physical tests (Fig. 1c). Previous studies have shown that the blood cell composition changes with aging, characterized by an increase in myeloid cells and a corresponding decrease in

lymphoid cells.^{41,42} Notably, mice transplanted with young HSCs exhibited a more youthful blood cell composition, characterized by increased B cell and reduced T cell and myeloid cell proportions, as well as an increase in overall white blood cells and lymphoid counts, compared to the recipients that received old HSCs (Fig. 1d, e). This suggests a crucial role of HSCs in systematic hematopoietic aging.

The ratio of naïve T cells serves as a critical indicator of immune function, which declines with aging.⁴³ Conversely, central memory T cells (Tcm) and effector memory T cells (Tem) exhibit an increase with aging,⁴⁴ which were confirmed by our study (Supplementary

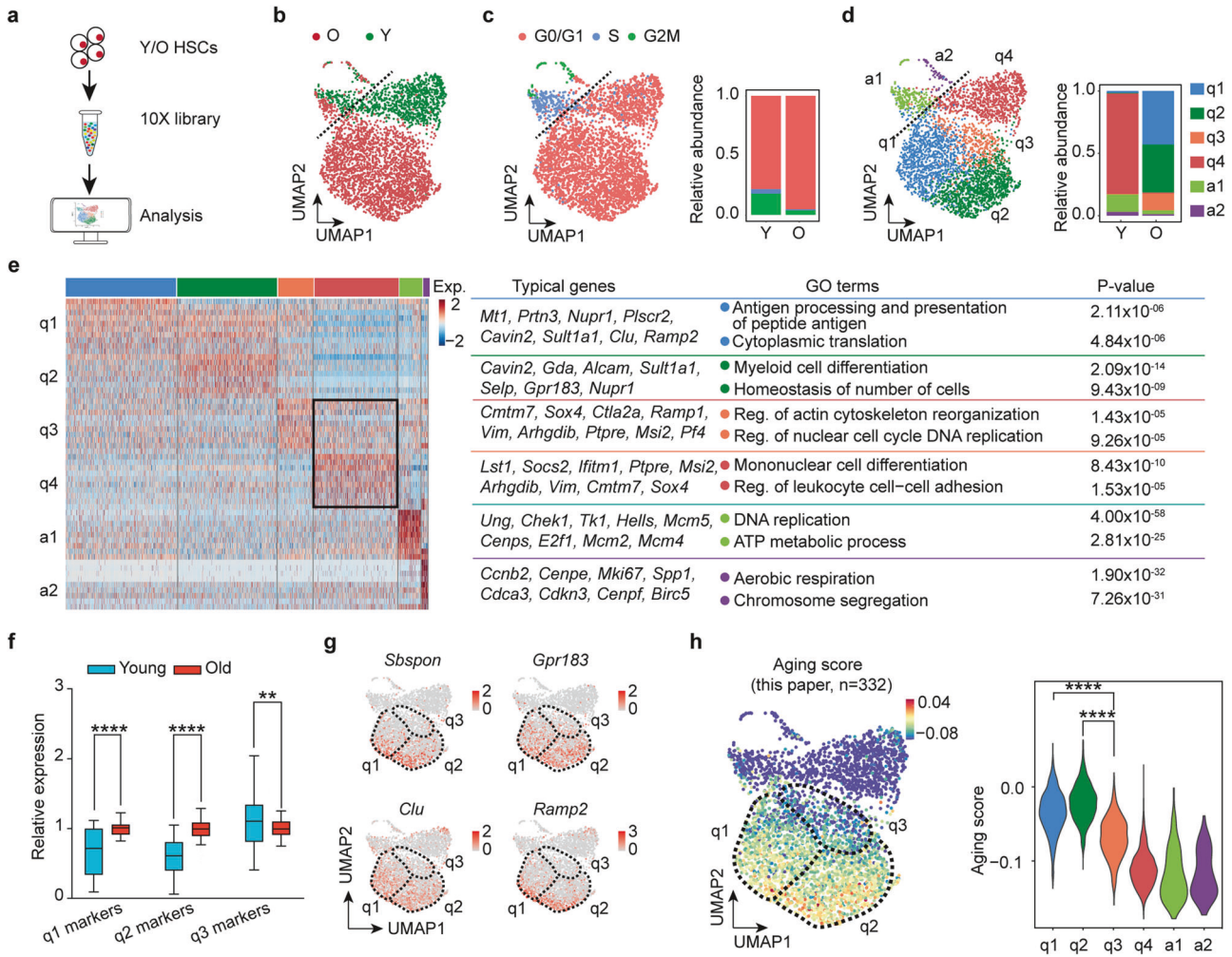


Fig. 2 scRNA-seq reveals increased heterogeneity of old HSCs. **a** Workflow of 10X scRNA-seq of young and old HSCs. The HSCs were sorted from young (2–3 months) and old (23 months) mice. **b** UMAP plot showing the distribution of young and old HSCs based on scRNA-seq. Clear separation of young and old HSCs indicates transcriptional changes of HSCs during aging. **c** Cell cycle phase analysis of young and old HSCs based on scRNA-seq. The S-phase and G2/M-phase marker genes are from Seurat package (V4.0.2). The cell cycle phase is determined by the relative expression levels of these marker genes. If neither S-phase nor G2/M phase genes are expressed, they are classified as G0/G1 phase. **d** UMAP plot showing unsupervised clustering of young and old HSCs. In total, 6 clusters were identified with two clusters (a1 and a2) representing active, and four clusters (q1–q4) representing quiescent cells. **e** Heatmap showing the cluster-specific marker genes expression across the 6 clusters and their enriched GO terms. Differentially expressed genes with $\text{min.pct} = 0.25$, $\text{logfc.threshold} = 0.25$ among the 6 clusters were used to generate the heatmap. Well-known HSC aging-related genes in clusters q1 and q2 are highlighted. Commonly identified marker genes in clusters q3 and q4 were also highlighted. Exp., expression; Reg., regulation. **f** Box plot showing relative expression of marker genes of q1, q2 and q3 in young and old HSCs via analysis of bulk RNA-seq. The expression level was normalized to the average expression level of the old. Plot shows the mean and 5–95 percentile. Two-sided unpaired Wilcoxon test. **g** UMAP presentation of the well-known HSC aging marker genes, *Sbspon*, *Gpr183*, *Clu* and *Ramp2* in each of the single cells. **h** UMAP plot and violin plot showing the calculated aging score of single cells of different clusters based on the HSC aging genes identified in bulk RNA-seq. In total, 332 upregulated genes in old HSCs were used for aging score calculation. Two-sided unpaired Wilcoxon test. $**P < 0.01$, $****P < 0.0001$.

information, Fig. S2). Notably, the old mice that received young HSCs have more naïve T cells in both CD4 and CD8 T cells (Fig. 1f; Supplementary information, Fig. S3a, b), indicating an improved immune system after receiving young HSCs transplantation.

The DNA methylation clock is widely used as an indicator of aging.⁴⁵ Importantly, old mice that received young HSCs have a younger epigenetic age in blood compared to those that received old HSCs (Fig. 1g). Consistently, old mice that received young HSCs exhibited improved physical functions compared to those that received aged HSCs, including muscle strength, motor coordination, locomotor activity and cognitive functions (Fig. 1h), without significant difference in body weight and spatial memory (Supplementary information, Fig. S3c–e). Collectively, these results demonstrate that transplantation of young HSCs to old mice can alleviate aging-related phenotypes.

scRNA-seq reveals a “younger” HSC subpopulation in old mice

The above results suggest that HSCs from old mice are functionally defective compared to those from young mice. To understand the defects, we performed both bulk RNA-seq and scRNA-seq on young and old HSCs (Fig. 2a), which revealed a clear transcriptomic difference between young and old HSCs (Fig. 2b; Supplementary information, Fig. S4a). Bulk RNA-seq revealed 332 upregulated genes in old HSCs, including previously annotated HSC aging marker genes,⁴⁶ including *Clu*, *Selp*, *Mt1* and *Ramp2* (Supplementary information, Fig. S4a and Table S1). These genes were defined as HSC aging marker genes for downstream analysis. Interestingly, unsupervised clustering analysis of scRNA-seq revealed that while the quiescent young HSCs are largely uniform, the quiescent old HSCs can be further divided into 3 clusters (q1–q3) (Fig. 2c, d). This result indicates that quiescent old HSCs

are transcriptionally more heterogeneous compared to young HSCs.

We then identified the marker genes for different clusters (Fig. 2e; Supplementary information, Table S2). Intriguingly, although q1–q3 are all from old HSCs, the known aging marker genes, such as *Mt1*, *Nupr1*, *Cavin2*, *Clu*, *Ramp2*, *Alcam*, *Selp* and *Gpr183*, are highly expressed in q1 and q2 clusters, but not in q3 cluster (Fig. 2e). In contrast, q3 and q4 (young HSCs) clusters share highly expressed genes, despite the q3 cluster originating from old mice. Gene Ontology (GO) analysis of q3 marker genes revealed an enrichment of cell proliferation-related pathways (Fig. 2e), which were also enriched in the young HSCs (Supplementary information, Fig. S4b, aging-down). We further calculated the relative expression levels of q1, q2, and q3 marker genes in old and young HSCs, and found that the q1 and q2 marker genes are expressed significantly higher in old HSCs, while q3 marker genes are higher in young HSCs (Fig. 2f), supporting a younger transcriptome of q3 HSCs.

To gain further support for the notion that a subset of HSCs from old mice are “younger” in their transcriptome, we analyzed the UMAP distribution of some well-known HSC aging marker genes (*Sbspon*, *Gpr183*, *Clu*, *Ramp2*)⁴⁶ and found that they are expressed at a higher level in q1 and q2 compared to that in q3 (Fig. 2g). In contrast, the young HSC marker genes, such as *Rnase6* and *Arhgap30*, exhibited an opposite expression pattern (Supplementary information, Fig. S4c). To quantify the aging heterogeneity of old HSCs, we calculated the aging score using the 332 HSC aging marker genes (Supplementary information, Table S1) or the top 100 reported HSCs aging genes (Supplementary information, Table S3).⁴⁶ Both analyses indicate that cluster q3 has a lower aging score than q1 and q2, despite all cells originating from the same old mice (Fig. 2h; Supplementary information, Fig. S4d). Collectively, comparative scRNA-seq analysis revealed increased aging heterogeneity in old HSCs and a subset of old HSCs that have a younger transcriptome.

CD150 can serve as an aging heterogeneity marker for old HSCs

To better understand the aging heterogeneity of old HSCs and to assess its contribution to overall body aging, a unique cell surface marker that facilitates the separation of “younger” from “older” cells in aged HSCs is needed. To this end, we first identified the top 150 genes showing strong correlation with aging scores in scRNA-seq (Supplementary information, Fig. S5a) and compared them with the 332 genes upregulated in old HSCs (Supplementary information, Fig. S4a), resulting in 54 shared genes (Fig. 3a; Supplementary information, Table S4). We further required membrane location for sorting purposes, which reduced the candidate gene list to 26 (Fig. 3a). Furthermore, the potential marker genes should have lower expression levels in q3 than in q1 and q2, which further narrowed the list to 7 (Supplementary information, Fig. S5b). Considering the availability and specificity of the antibodies, CD150 (*Slamf1*) was selected as the marker for aging heterogeneity of old HSCs. FACS analysis of HSCs from young and old mice indicated that the population of HSCs with higher CD150 levels significantly increases with aging (Fig. 3b), supporting the use of CD150 as an indicator of aging heterogeneity in old HSCs.

To further confirm that the CD150 level can serve as a marker of aging heterogeneity of old HSCs, we separated old HSCs into 4 groups (G1 to G4) by FACS based on CD150 levels and profiled their transcriptomes (Fig. 3c). We then calculated the expression correlation between CD150 and each gene and identified 131 and 103 genes that exhibit strong positive or negative correlation with CD150 in aged HSCs, respectively (Supplementary information, Fig. S5c and Table S5). Notably, the genes that positively correlate with CD150 include many known HSC aging markers, including *Sbspon*, *Ehd3*, *Clu*, *Selp*, *Jam2* and *Enpp5*. In contrast, the negatively

correlated genes include genes that are highly expressed in young HSCs, such as *Serp1b1a*, *Usp6nl*, *Lrr1* and *Kif15* (Supplementary information, Fig. S5d). These results suggest that CD150 level can be a potential indicator of HSC transcriptome age.

Using the 131 genes that positively correlate with the CD150 level (referred to as CD150 feature genes), we calculated the CD150 feature score and found that q3 HSCs have a significantly lower CD150 feature score than q1 and q2 HSCs (Supplementary information, Fig. S5e, f). Notably, a strong correlation between the CD150 feature score and aging score was observed (Fig. 3d). This indicates that the aging heterogeneity of old HSCs can be well reflected by CD150 feature genes. Consistently, HSC aging-related up- and down-regulated genes in the 4 groups of HSCs from G1 to G4 exhibit a trend that is similar to the aging process (Fig. 3e), confirming the positive correlation between CD150 level and HSC aging status in old mice.

CD150^{low} HSCs from old mice have younger epigenome and superior functions

Epigenetic changes are believed to be one of the drivers of aging.^{47–49} To further determine whether CD150 level can reflect epigenetic aging in old HSCs, we first compared their epigenetic age and found that CD150^{low} HSCs have a lower epigenetic age than that of CD150^{high} HSCs despite that they are from the same old mice (Fig. 3f). Given that stem cell aging is accompanied by chromatin accessibility changes,^{50–52} we compared the chromatin accessibility landscapes of old CD150^{low} and CD150^{high} HSCs, as well as young and old HSCs by performing ATAC-seq analyses. We found that 4694 peaks displayed increased chromatin accessibility and 3842 peaks showed decreased accessibility in aged HSCs relative to young HSCs, while 3066 open and 1966 closed differential peaks were identified between old CD150^{low} and CD150^{high} HSCs (Supplementary information, Fig. S5g, h). Interestingly, a similar change between CD150^{low} and CD150^{high} old HSCs was also observed around the aging-related ATAC-seq peaks (Fig. 3g). These results indicate that CD150 can serve as a marker reflecting both transcriptional and epigenetic aging in aged HSCs.

When we further checked the genes close to the differential accessible peaks, we found several HSC aging-related genes, including *Clu*, *Jam2*, *Mt2*, *Nupr1*, *Selp*, *Slamf1* (CD150) and *Vwf*, are located near the aging-related open peaks, and these genes also harbor the open peaks when comparing old CD150^{high} and CD150^{low} HSCs (Supplementary information, Fig. S5g, h). Consistently, the genes located around closed differential accessible peaks in both comparisons include many highly expressed genes in young HSCs, such as *Cd52*, *Cdc6*, *Haao* and *Nkg7*, demonstrating the corresponding chromatin accessibility changes underlying transcriptome alteration.

In addition, GO analysis of the genes related to the differential accessible peaks revealed enrichment of ‘cell adhesion’ and ‘potassium transport’ in the open peaks in both comparisons (Supplementary information, Fig. S5g, h). Previous studies have demonstrated a correlation between ‘cell adhesion’ with HSCs functions and aging,^{46,53,54} further supporting the potential functional defects in old and CD150^{high} HSCs compared to their counterparts.

To gain further insight into the aging-related open and closed ATAC-seq peaks, we performed motif enrichment analysis. We found that the aging-related open peaks are enriched for binding sites of the AP-1 family transcription factors (TFs), while the aging-related closed peaks are enriched for the E26 transformation-specific (ETS) family TFs, including SPIB and PU.1 (Supplementary information, Fig. S5i). Importantly, similar TFs were identified when comparing CD150^{low} and CD150^{high} old HSCs (Supplementary information, Fig. S5j), further supporting a relatively younger chromatin in old CD150^{low} HSCs compared to the CD150^{high} HSCs. AP-1 family TFs have been reported as pioneer factors in aging,^{55,56} while PU.1 and SPIB play important roles in regulating

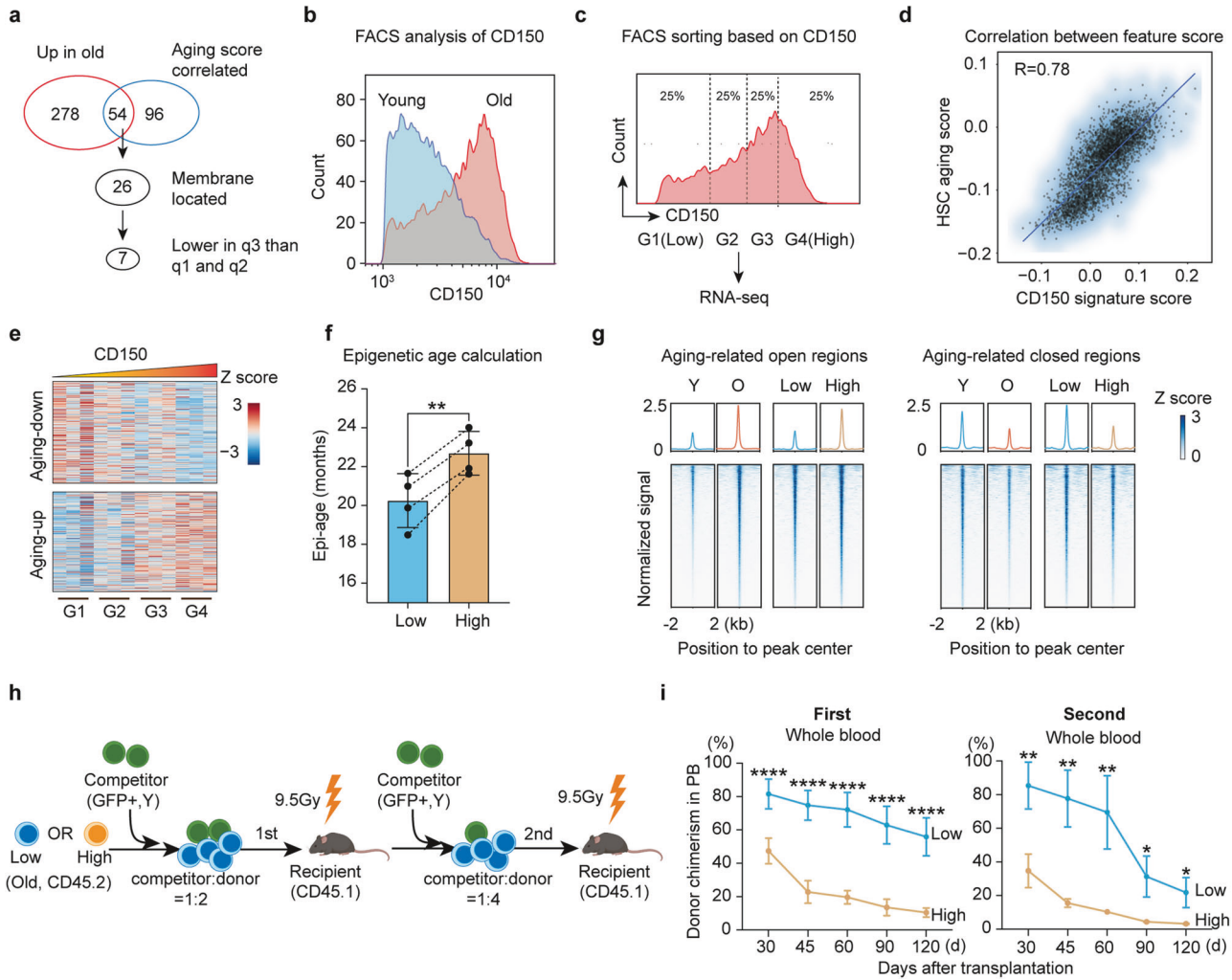


Fig. 3 Identification of CD150 as an HSC aging heterogeneity marker. **a** Workflow for identifying heterogeneity marker genes in old HSCs. **b** FACS plot showing expression level of CD150 in young (3 months) and old (22–24 months) HSCs. **c** HSCs from old mice were separated into four subgroups (25% for each) based on their CD150 protein levels and subjected to bulk RNA-seq, $n = 3$. **d** Dot plot showing Pearson correlation between CD150 signature score and aging score based on scRNA-seq data, $R = 0.78$. **e** Heatmap showing changes in expression of aging-related genes with ascending level of CD150 based on bulk RNA-seq in **c**. **f** Bar plot showing the epigenetic age of CD150^{low} and CD150^{high} HSCs from 22- to 24-month-old mice, $n = 4$, paired t -test. The HSC subsets from the same mice were paired with dashed line. **g** Line plot and heatmap showing ATAC-seq signal difference between CD150^{low} and CD150^{high} HSCs in aging-related open and closed regions, respectively. **h** Diagram of competitive transplantation to evaluate the repopulation capacity of CD150^{low} and CD150^{high} HSCs from old mice. **i** Whole blood chimerism of CD150^{low} and CD150^{high} HSCs from 22- to 24-month-old donor mice at different time points after the 1st and 2nd transplantation, $n = 6$ for the first and $n = 3$ for the second transplantation. Mean \pm SD, Student's t -test, * $P < 0.05$, ** $P < 0.01$, **** $P < 0.0001$. The graphic of the mouse in **h** was created with BioRender.

hematopoiesis,^{57,58} further highlighting the altered chromatin status and potentially impaired functions in the old CD150^{high} HSCs.

Previous studies have shown that increased DNA damage and decreased percentage of cells in proliferation are associated with functional decline of old HSCs.^{27,59,60} Interestingly, we observed an increase of double stranded breaks (indicated by γ H2AX) as well as a decrease in the proportion of cells in proliferation in CD150^{high} compared to CD150^{low} old HSCs (Supplementary information, Fig. S5k, l), indicating that CD150^{low} HSCs may have better functions than CD150^{high} HSCs in old mice.

To directly compare the functions between old CD150^{low} and CD150^{high} HSCs, we performed serial competitive transplantation (Fig. 3h). We found that CD150^{low} old HSCs have significantly better engraftment capacity compared to their CD150^{high} counterparts in both the first and second transplantation (Fig. 3i; Supplementary information, Fig. S6a, b). These results

demonstrate that CD150 level not only marks transcriptome and epigenome heterogeneity, but also reflects functional heterogeneity of old HSCs.

Despite old CD150^{low} HSCs being molecularly and functionally younger than CD150^{high} HSCs, the extent to which they are similar to young HSCs remains unclear. To this end, we conducted molecular and functional comparisons between young HSCs and old CD150^{low} HSCs. The transcriptome comparison showed that, although old CD150^{low} HSCs are younger than CD150^{high} HSCs, they are still different from young HSCs in the expression of aging-related genes (Supplementary information, Fig. S6c). In terms of chromatin accessibility, old CD150^{low} HSCs are similar to young HSCs in aging-related closed regions but have higher signals in aging-related open regions (Supplementary information, Fig. S6d). These results demonstrate that old CD150^{low} HSCs are younger than old CD150^{high} HSCs, but still older than young HSCs at the molecular level. As for the direct functional comparison, based on

the competitive transplantation experiment (Fig. 3h), we found that old CD150^{low} HSCs retain about 72.9% functionality relative to that of the young HSCs in terms of their repopulation capability, while the old CD150^{high} HSCs only retain about 5.9% (Supplementary information, Fig. S6e). Collectively, these results indicate that although old CD150^{low} HSCs are not as youthful as young HSCs at the molecular and functional levels, they retain most of the functionality of young HSCs.

Although young HSCs exhibit a homogeneous transcriptome (Fig. 2d) and aging score (Fig. 2h), their CD150 levels are variable (Fig. 3b). This raised the question whether CD150^{low} HSCs are also functionally superior to CD150^{high} HSCs in young mice. To address this question, we checked the cell cycle and performed similar HSC transplantation experiments using young HSCs (Supplementary information, Fig. S7a, b). Consistent with their transcriptome and aging score homogeneity, no significant functional difference was observed between CD150^{low} and CD150^{high} young HSCs for cell cycle analysis or peripheral blood (PB) chimerism during the period of 120 days after transplantation (Supplementary information, Fig. S7a–d). However, we noted a myeloid bias and significantly higher contribution to myeloid cells in young CD150^{high} HSCs, along with an upward trend in PB chimerism when compared to CD150^{low} young HSCs (Supplementary information, Fig. S7c, d). These results indicate that CD150^{high} HSCs from young mice have comparable or even better functions compared to CD150^{low} HSCs, which is in contrast to those in old mice. Furthermore, these findings also suggest that myeloid-biased differentiation is not linked to aging status or decreased functionality in young HSCs.

Old CD150^{high} HSCs are defective in differentiation, but not in self-renewal or activation

We next attempted to dissect the mechanism underlying the differential repopulation capacity of CD150^{low} and CD150^{high} HSCs in old mice. Considering that self-renewal and differentiation are the two major features of stem cells, we compared both features after their transplantation. We first determined the differentiation dynamics of old HSCs at different time points after transplantation (Supplementary information, Fig. S8a). We found that transplanted old HSCs start to differentiate on day 7, and the progenitor subpopulation becomes apparent on day 10 (Supplementary information, Fig. S8b). Based on this, we separately transplanted old CD150^{low} and CD150^{high} HSCs and analyzed the donor-derived hematopoietic stem and progenitor cells (HSPCs) in bone marrow on days 7 and 14 after transplantation (Fig. 4a). Notably, we found that CD150^{high} HSCs showed a significantly lower ratio in short term HSCs (ST-HSCs) and multipotent progenitors (MPPs), but a higher ratio in LT-HSCs compared to CD150^{low} HSCs (Fig. 4b; Supplementary information, Fig. S8c), indicating that old CD150^{high} HSCs might have differentiation and/or activation defects.

To distinguish between these two possibilities, we profiled transcriptomes of CD150^{low} and CD150^{high} HSCs 4 days after transplantation when the HSCs had yet to initiate differentiation (Supplementary information, Fig. S8d). By comparing with freshly isolated HSCs, we identified 794 commonly upregulated genes in both CD150^{low} and CD150^{high} HSCs after transplantation (Supplementary information, Fig. S8e and Table S6). The commonly upregulated genes are highly enriched in terms related to cellular division. Consistently, the G2M checkpoint-related genes were similarly upregulated in both CD150^{low} and CD150^{high} HSCs upon transplantation (Supplementary information, Fig. S8f). These results indicate that old CD150^{high} HSCs can be effectively activated as that of CD150^{low} HSCs following transplantation.

We further compared the proliferation capacity of old CD150^{low} and CD150^{high} HSCs in culture and found that old CD150^{low} and CD150^{high} HSCs exhibited comparable proliferation rates (Supplementary information, Fig. S8g–k). Taken together, these results indicate that impaired repopulation capacity of old CD150^{high}

HSCs is caused by defective differentiation, but not activation or proliferation.

To rule out a possible delay in differentiation of old CD150^{high} HSCs after transplantation, we analyzed the persistence of the differentiation and self-renewal capacity of old CD150^{high} HSCs over an extended period of 5 months. We co-transplanted old CD150^{low} or CD150^{high} HSCs (GFP⁻) with competitors (GFP⁺) and analyzed the differentiation and chimerism of donor HSCs 5 months later (Fig. 4c). We observed a consistent differentiation defect of old CD150^{high} HSCs when compared to their CD150^{low} counterparts by analyzing donor-derived HSPCs in the bone marrow (Fig. 4d). Additionally, the donor chimerism of old CD150^{high} HSCs exhibits a clear trend of decline from LT-HSCs through ST-HSCs, MPPs, to PB, while the donor chimerism of old CD150^{low} HSCs remains relatively stable (Fig. 4e), supporting a long-term differentiation defect of old CD150^{high} HSCs.

Collectively, these results indicate a long-lasting impairment in differentiation, but not in activation or self-renewal of old CD150^{high} HSCs.

Old CD150^{high} HSCs are defective in the LT-HSCs to ST-HSCs transition

To determine the specific stage when the differentiation defects of old CD150^{high} HSCs occur, we performed comparative scRNA-seq analysis of the HSPCs derived from old CD150^{low} and CD150^{high} HSCs 14 days after transplantation. We obtained 2406 and 1925 high quality HSPCs derived from transplanted CD150^{low} and CD150^{high} HSCs, respectively (Fig. 4f). Cell cycle phase analysis indicated that similar proportions of HSPCs derived from CD150^{low} and CD150^{high} HSCs were actively cycling (Supplementary information, Fig. S9a), consistent with our previous results (Supplementary information, Fig. S8e, f).

Based on the expression of the HSPC marker genes^{50,61} and the HSPC sorting markers (*Ly6a*, *Kit*, *Cd34*, *Cd48* and *Slamf1*), the 4331 HSPCs can be divided into 7 subclusters that include LT-HSC-like, ST-HSC-like, MPP2-like, MPP3-like, MPP4-like, GMP-like and MEP-like cells (Fig. 4g; Supplementary information, Fig. S9b). When HSPCs derived from CD150^{low} and CD150^{high} HSCs were compared, we found that HSPCs derived from CD150^{high} HSCs were significantly enriched in LT-HSC-like cells (Fig. 4g, h), consistent with our FACS analysis (Fig. 4b; Supplementary information, Fig. S8c). Since the proportions of CD150^{low} and CD150^{high} HSCs-derived ST-HSCs are comparable, our data indicate that the differentiation defects of CD150^{high} HSCs were mainly at the stages of LT-HSC to ST-HSC, and ST-HSC to MPP4 transitions. Given that MPP4 are the major progenitor cells of the lymphoid lineage, the substantial decrease in the MPP4 population might be a major cause of the biased differentiation of CD150^{high} HSCs.^{30,32}

Consistently, when we further performed pseudo time analysis to map the differentiation trajectory, we found that HSPCs derived from CD150^{high} HSCs were predominantly enriched at early stages and less enriched at later stages compared to HSPCs derived from old CD150^{low} HSCs (Supplementary information, Fig. S9c), supporting that the differentiation of CD150^{high} HSCs is impaired compared to their CD150^{low} counterparts.

To further analyze the transcriptome differences between populations derived from old CD150^{low} and CD150^{high} HSCs, we identified differentially expressed genes between them. Significant transcriptome differences were observed in LT-HSC-like, ST-HSC-like, and MPP4-like subpopulations (Supplementary information, Fig. S9d–f). Interestingly, some HSC aging marker genes, such as *Vwf*, *Nupr1*, *Ilfm3*, and *Ilfm1* are consistently upregulated in HSPCs derived from old CD150^{high} HSCs, indicating that upregulation of HSC aging genes can persist in downstream cells.

To further investigate the transcriptome difference, we performed GO analysis. Upregulated genes in cells derived from CD150^{low} HSCs are consistently enriched for 'translation-related

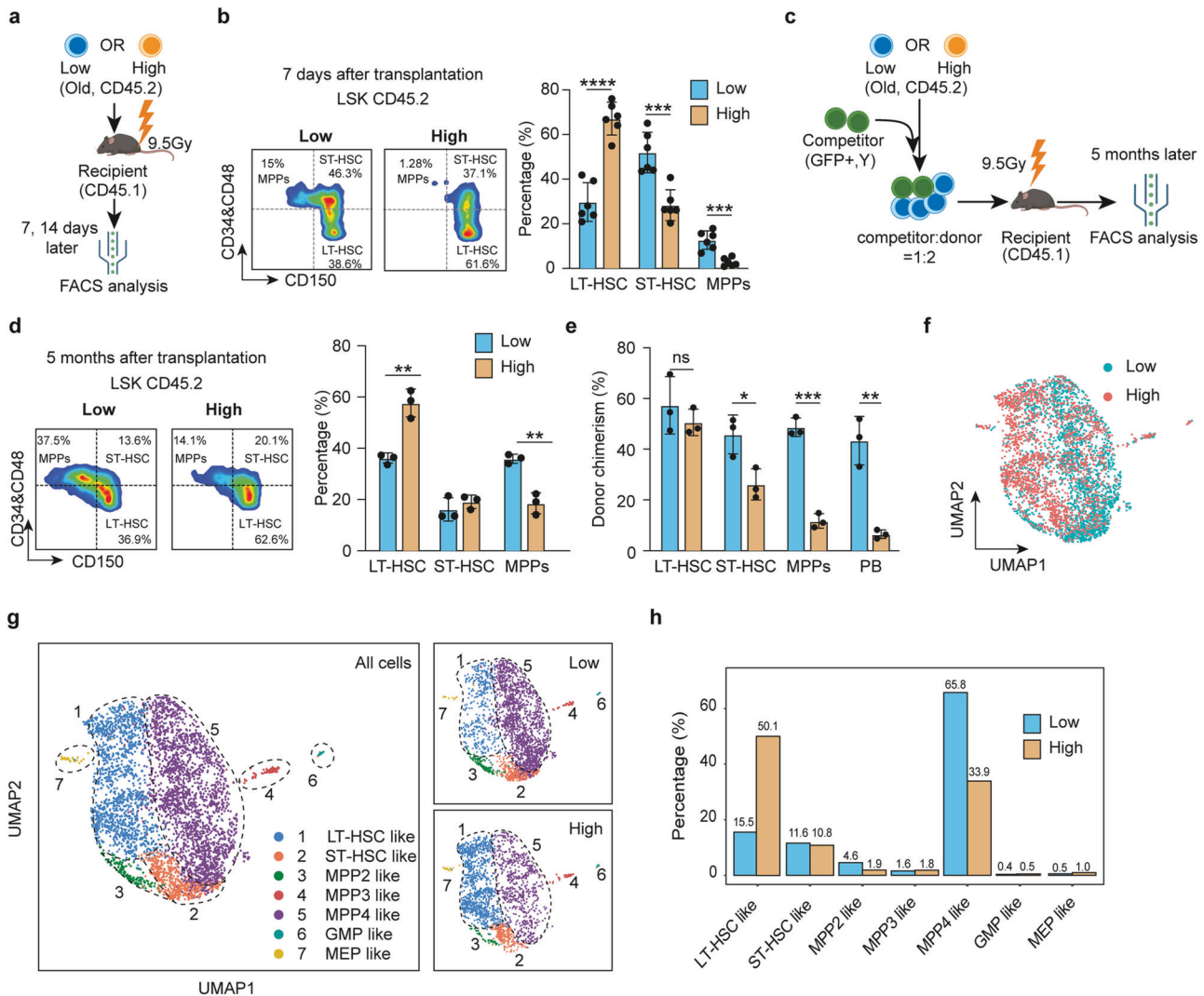


Fig. 4 Differentiation, but not self-renewal, is a major defect of old CD150^{high} HSCs. **a** Diagram illustration of the transplantation experiment comparing old CD150^{low} and CD150^{high} HSCs. Donor HSCs-derived HSPCs from the bone marrow were analyzed on days 7 and 14 after transplantation. **b** Representative FACS analysis of donor HSCs-derived HSPCs (left) and quantification of different cell populations 7 days after transplantation (right). LT-HSC (CD45.2 LSK, CD34⁺CD48⁻CD150⁺), ST-HSC (CD45.2 LSK, CD34⁺CD48⁺CD150⁺) and MPPs (CD45.2 LSK, CD34⁺CD48⁺CD150⁻) were analyzed, $n = 3$. **c** Diagram illustration of the competitive transplantation for evaluating the long-term differentiation of CD150^{high} HSCs. Both PB and bone marrow were analyzed five months after transplantation. **d** Representative FACS analysis of donor HSC-derived HSPCs (left) and quantification of different cell populations (right) 5 months after transplantation, $n = 3$. **e** Bar graph showing the chimerism of donor HSCs in LT-HSCs, ST-HSCs, MPPs and PB 5 months after transplantation, $n = 3$. **f** UMAP plot showing cell distribution of HSPCs derived from CD150^{low} and CD150^{high} HSCs in scRNA-seq 14 days after transplantation. **g** UMAP presentation of cell types predicted based on HSPC marker gene expression (left). In total, 7 different cell types were identified in HSPCs. **h** Bar graph showing relative abundance of predicted cell types in HSPCs from mice that received old CD150^{low} or CD150^{high} HSCs. Mean \pm SD, Student's t -test, $*P < 0.05$, $**P < 0.01$, $***P < 0.001$. The graphics of the mouse in **a** and **c** were created with BioRender.

pathways' across cell types, while those from CD150^{high} HSCs are enriched for 'protein folding response-related pathways' (Supplementary information, Fig. S9g). Increased translation in HSCs is associated with differentiation activities,^{62–64} indicating more active differentiation in old CD150^{low} HSCs. Protein folding response is linked to cellular stress, a hallmark of HSC aging,^{65,66} consistent with the impaired functions of old CD150^{high} HSCs. The consistently enriched pathways among cell types indicate that transcriptomic defects in HSCs may be passed to downstream progenitors.

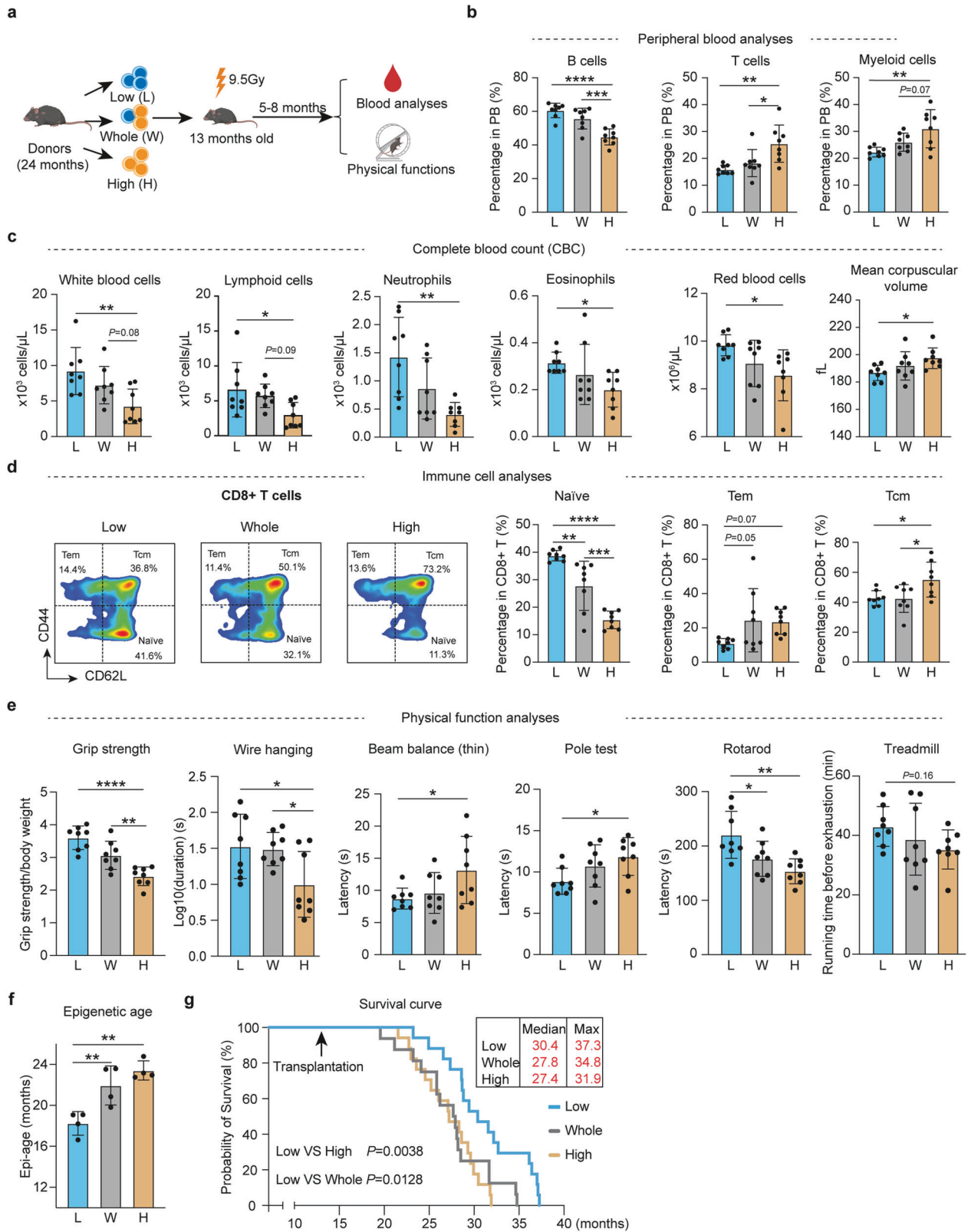
To gain further support for this notion, we performed Gene Set Enrichment Analysis (GSEA) comparing HSPCs from old CD150^{low} and CD150^{high} HSCs. Several pathways are consistently enriched in cells derived from old CD150^{high} HSCs, including IFN- α response, mTOR signaling, unfolded protein response, and glycolysis

(Supplementary information, Fig. S9h). Some of these pathways have been linked to stem cell aging and their differentiation activities,^{66–69} further supporting that transcriptome defects in HSCs can be passed on to downstream cells.

Collectively, comparative bone marrow scRNA-seq analysis of transplanted old HSCs indicated that the differentiation defects of old CD150^{high} HSCs is caused by a block of LT-HSCs to ST-HSCs transition and the transcriptome defects of HSCs can be passed on to downstream progenitor cells.

The "younger" subset of old HSCs can alleviate aging phenotypes and extend lifespan

Transplantation of young HSCs as an anti-aging therapy is impractical for humans due to immune incompatibility among different individuals. Given this challenge, the demonstration that



HSCs in old mice have molecularly and functionally “younger” CD150^{low} HSCs prompted us to ask whether this subset of HSCs can help to attenuate aging phenotypes of old mice. To this end, we transplanted CD150^{low}, whole HSCs (un-selected), or CD150^{high} HSCs from old mice into 13-month-old recipients and analyzed

aging phenotypes 5 months later (Fig. 5a). Compared to mice that received CD150^{high} HSCs, mice transplanted with CD150^{low} HSCs showed higher percentage of B cells, and lower percentage of T cells and myeloid cells (Fig. 5b), as well as increased blood cell numbers, including lymphoid cells, neutrophils, eosinophils and

Fig. 5 Transplantation of “younger” subset of old HSCs alleviates aging phenotypes of aged mice. **a** Diagram showing the experiment design of individual transplantation of 2000 old CD150^{low} (25% lowest), whole-HSCs (un-selected) and CD150^{high} (25% highest) HSCs into middle-aged recipients (13-month-old), $n = 8$. Five months after transplantation, a series of hematopoietic and physical tests were performed. **b** Bar graph showing the percentage of B, T and myeloid cells in the PB of recipient mice of the three groups, $n = 8$. **c** Bar graph showing absolute number of blood cells in PB of recipient mice from different transplanted groups, $n = 8$. **d** Representative FACS analysis of naïve T cells, Tcm and Tem ratio in CD8⁺ T cells and their quantification in recipient mice of the three groups, $n = 8$. **e** Physical tests of recipient mice that received CD150^{low}, whole-HSCs and CD150^{high} HSCs. Muscle strength, motor coordination and endurance were assessed, $n = 8$. **f** Bar graph showing the epigenetic age of recipient mice from different groups using blood samples, $n = 4$. **g** Survival curve showing the lifespan difference among mice that received old CD150^{low}, whole-HSCs and CD150^{high} HSCs. Each mouse received 2000 HSCs. Log-rank (Mantel-Cox) test, $n = 17$. For **b–f**, mean \pm SD, one-way ANOVA, * $P < 0.05$, ** $P < 0.01$, *** $P < 0.001$, **** $P < 0.0001$. The graphic of the mouse in **a** was created with BioRender.

red blood cells (Fig. 5c). Notably, a significant increase in naïve T cell ratio and a corresponding decrease in the Tcm and Tem cell ratios were observed when comparing mice that received old CD150^{low} HSCs to those that received old CD150^{high} HSCs (Fig. 5d; Supplementary information, Fig. S10a). These results suggest that transplantation of old CD150^{low} HSCs can improve both hematopoiesis and immune parameters in old recipient mice.

To determine whether improved hematopoiesis and immune functions can improve physical performance, we performed a series of tests that measure muscle strength (grip strength, wire hanging), coordination (beam balance, pole test), and endurance (rotarod and treadmill). Consistently, we found a general trend of degrading physical performance in the order of CD150^{low}, whole-HSCs, and CD150^{high} HSCs (Fig. 5e) without significant differences in their body weight (Supplementary information, Fig. S10b). Consistent with improved physical performance, we found that old mice that received CD150^{low} HSCs displayed a lower epigenetic age in blood (Fig. 5f). Importantly, aged recipient mice transplanted with old CD150^{low} HSCs exhibited a substantial lifespan extension, achieving a 9.4% and 11.5% increase in median lifespan, and a 7.2% and 16.9% increase in maximum lifespan compared to counterparts transplanted with whole-HSCs or CD150^{high} HSCs (Fig. 5g).

Taken together, our results indicate that not only transplantation of young HSCs, but the “younger” subset of old HSCs can attenuate aging phenotypes of old mice. Considering that the functionally defective CD150^{high} HSCs increase with aging, our study raises the possibility that aging-alleviating effects might be achieved by reducing or removing the functionally defective CD150^{high} HSCs from old mice.

Reducing the dysfunctional HSCs can alleviate aging phenotypes in old recipient mice

To assess whether reducing defective HSCs in old mice can enhance hematopoiesis and mitigate aging-related phenotypes, we mixed 500 old CD150^{low} HSCs with 2500 (1:5 ratio), 1000 (1:2 ratio) or 0 (1:0 ratio) CD150^{high} old HSCs and co-transplanted to irradiated middle-aged (13 months) mice to mimic whole-HSC, partial removal, and complete removal of CD150^{high} HSCs, respectively. Five months after the transplantation, we assessed the hematopoietic system and physical functions of recipient mice to compare the aging status of the three groups (Fig. 6a). The 1:5 ratio serves as a control, which is determined based on the percentage of q3 to the total HSC in old mice based on scRNA-seq (Fig. 2d).

PB analyses indicated that compared to the 1:5 group, the 1:2 and 1:0 groups have increased percentage of B cells and decreased percentage of myeloid cells (Fig. 6b). Complete blood counting also showed higher number of whole white blood cells, neutrophils, and lymphoid cells in the 1:0 and 1:2 groups compared to the 1:5 group (Fig. 6c). Importantly, increased naïve CD4⁺ and CD8⁺ T cells, as well as decreased effective memory T cells were also detected in the 1:2 and 1:0 groups compared to the 1:5 group (Fig. 6d; Supplementary information, Fig. S11a), indicating that the presence of the defective CD150^{high} HSCs has

adverse effects on the “younger” functional CD150^{low} HSCs for hematopoiesis and immune function in old mice.

Next, we examined whether reducing the CD150^{high} HSCs ratio can improve physical functions of the recipient mice by performing a multitude of physical tests. The results indicate consistent improved physical functions in the 1:2 and 1:0 groups compared to the 1:5 group, including muscle strength (grip strength), motor coordination (pole test, beam balance, and rotarod), and locomotor activity (open field test), with no notable differences in body weight (Fig. 6e; Supplementary information, Fig. S11b). These findings not only confirm the adverse effect of the defective CD150^{high} HSCs in aged mice, but also suggest that their reduction in old mice can ameliorate aging-related phenotypes.

DISCUSSION

By transplantation, we demonstrated a key role of HSCs in systematic aging. Integrating scRNA-seq and functional evaluation, we identified a “younger” subset of HSCs in old mice that is marked by low level of CD150. Comparative analysis demonstrated that CD150^{high} HSCs from old mice are defective in LT-HSC to ST-HSC differentiation compared to the CD150^{low} HSCs. Importantly, transplantation of the “younger” CD150^{low} HSCs can alleviate aging phenotypes and extend the lifespan of old mice. Finally, we provide evidence demonstrating that the hematopoietic system and physical performance of old recipient mice can be improved by reducing the ratio of functionally defective CD150^{high} HSCs, raising the possibility that rejuvenation can be achieved by removing the dysfunctional HSCs in the elderly.

Originally characterized as a cell surface marker for LT-HSCs,⁷⁰ CD150 has also been used to reflect differentiation bias of HSCs in young and old mice.^{30,32} Additionally, CD150^{low} HSCs from aged mice have been shown to retain normal lymphoid differentiation capacity when removed from the aged microenvironment.³⁴ These previous results suggest a potential link between CD150 levels and HSC function during aging and are in line with our results, which further support CD150 as a marker of HSC aging heterogeneity. In addition to CD150, we identified other cell surface protein-coding genes, such as *Ramp2*, *Ehd3*, *EfnA1*, *Gpr183*, *Jam2*, and *Tm4sf1*, as potential markers of aging heterogeneity in old HSCs. Since all these markers were identified using the same criteria and they exhibit strong positive correlations with each other in expression (data not shown), we believe that they would segregate old HSCs into very similar populations. We chose to use CD150 over the others due to the availability of antibodies and their performance on old HSCs sorting (data not shown). Interestingly, during the preparation of this manuscript, Kim et al. reported that *Clca3a1* can also serve as a marker to capture the HSC heterogeneity in old mice. They found that *Clca3a1*^{high} HSCs from aged mice have a decreased repopulation capacity in primary transplantation and exhibit a myeloid-biased differentiation compared to *Clca3a1*^{low} HSCs.³¹ However, this functional difference between *Clca3a1*^{high} and *Clca3a1*^{low} old HSCs was not maintained in the second transplantation. In contrast, the

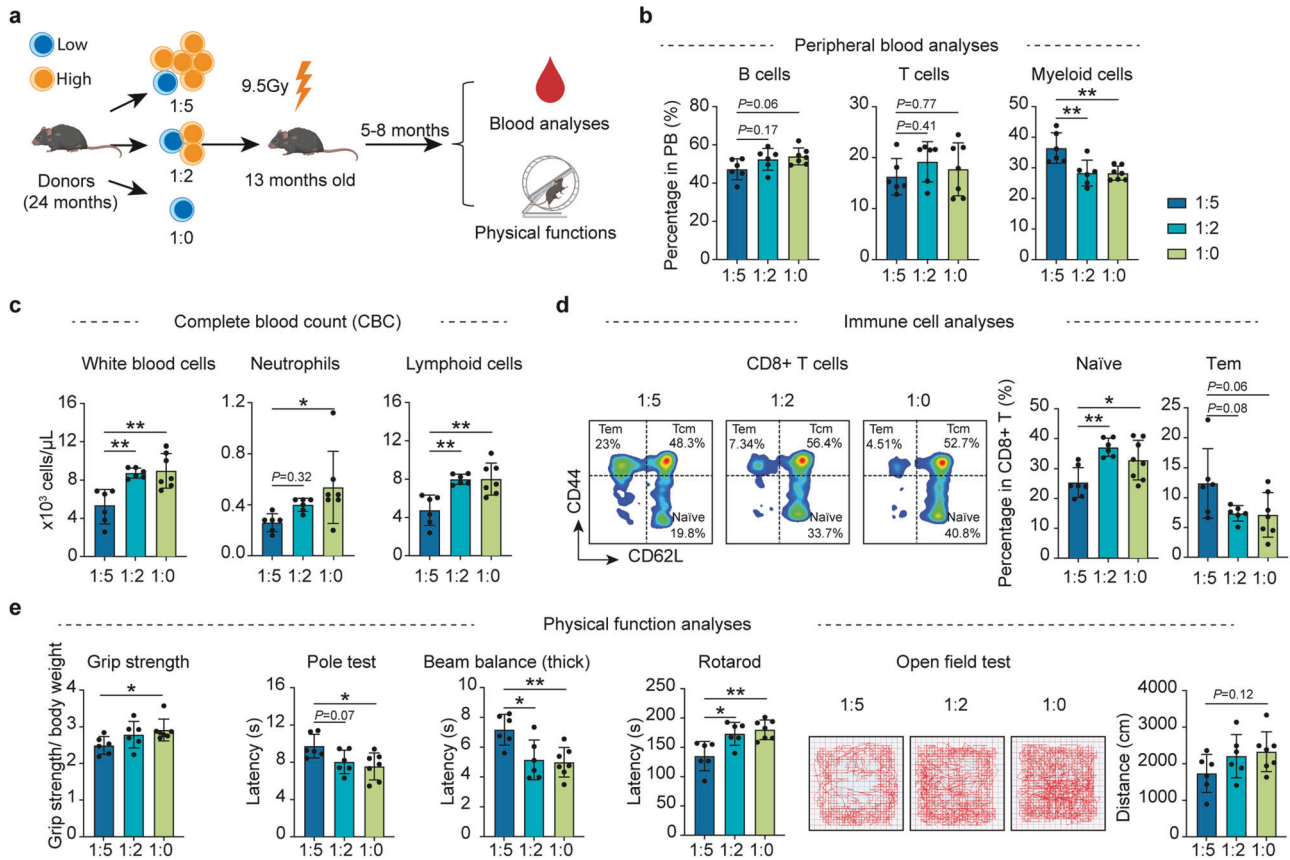


Fig. 6 Reducing dysfunctional HSCs ameliorates aging phenotypes in old mice after transplantation. **a** Diagram showing the experiment design. Individual transplantation of 500 old CD150^{low} HSCs with: 2500 CD150^{high} HSCs (1:5 group); 1000 CD150^{high} HSCs (1:2 group) and 0 CD150^{high} HSCs (1:0 group) into middle-aged recipients (13-month-old). Five months after transplantation, a series of hematopoietic and physical tests were performed. **b** Bar graph showing the percentage of B, T and myeloid cells in the PB of recipient mice of the different groups. **c** Bar graph showing the blood cell numbers in PB of recipient mice from different transplanted groups. **d** Representative FACS analysis of naive T cells and Tem ratio in CD8⁺ T cells and their quantification in recipient mice of different groups. **e** Bar plot showing the results of physical functional tests of recipient mice of different groups. Muscle strength, motor coordination, endurance and locomotor activity were assessed. $n = 6$ for 1:5 and 1:2 group, $n = 7$ for 1:0 group, mean \pm SD, one-way ANOVA, $*P < 0.05$, $**P < 0.01$. The graphics of the mouse and equipment in **a** were created with BioRender.

functional difference between CD150^{high} and CD150^{low} old HSCs persist in the second transplantation, indicating that CD150 is a more robust indicator of the functional heterogeneity of aged HSCs.

Since the discovery of the rejuvenating effects of young blood through parabiosis,⁷ great efforts have been made on searching for the rejuvenation factors from young blood. Although modulations of several candidate factors, such as CDC42, SELP, CCL5, PHF6, IGF1, PF4 and the Yamanaka factors (OCT4, SOX2, KLF4, c-MYC) have been reported to have rejuvenating effects during the past years,^{23,46,71–77} their rejuvenating capacities are limited and the mechanisms underlying their rejuvenating effects are not clear. In some cases, such as GDF11, conflicting results were also reported.^{9,10,78,79} Thus far, no universally accepted rejuvenating factors have been identified. Our findings reveal that old HSCs exhibit molecular and functional heterogeneity, comprising “younger” and dysfunctional “older” subsets. Moreover, reducing the proportion of dysfunctional HSCs ameliorates aging phenotypes in aged mice after transplantation, suggesting that removal of functionally defective HSCs from old could be a promising approach for alleviating aging phenotypes. Consistent with this notion, a very recent study showed that depletion of the myeloid-biased HSCs (marked by NEO1) by a specific antibody cocktail could restore immune functions in old mice,⁸⁰ although whether such approach can lead to a systemic body rejuvenation remains unknown. Nevertheless, our study and this

recent report have set the stage for achieving rejuvenation in the elderly by targeted removal of dysfunctional HSCs.

MATERIAL AND METHODS

Mouse

All experiments were conducted in accordance with the National Institute of Health Guide for Care and Use of Laboratory Animals and approved by the Institutional Animal Care and Use Committee (IACUC) of Boston Children’s Hospital and Harvard Medical School. For bulk and scRNA-seq, 2–3-month young and 22–24-month-old male C57BL/6 mice were used (Jackson Lab, #00664). For HSC transplantation, 2–3-month-old male young (Jackson Lab, #00664) or 2–3-month-old GFP⁺ male young (Jackson Lab, #006567) mice were used. For competitive transplantation, competitor HSCs were collected from 3–4-month GFP⁺ male young (Jackson Lab, #006567) mice. Except specially mentioned, the recipient mice were B6 CD45.1 male mice (Jackson Lab, #002014), and the helper cells were also collected from B6 CD45.1 male mice. For old recipient mice, 13-month-old wild-type male mice were used and the helper cells were from age-matched wild-type male mice.

LT-HSCs sorting and transplantation

Bone marrow cells were collected by crushing tibias, femurs, pelvic bone and spine. To improve the sorting efficiency, collected cells were further enriched by removing lineage-positive cells (CD4, CD8, Gr-1, CD11b, CD5, B220 and Ter119) with selection beads (STEMCELL, catalog #19856). The

enriched cells were further stained with antibodies against mouse c-Kit, Sca-1, CD48, CD34, CD150. The LT-HSCs were defined as Lin⁻Sca-1⁺c-Kit⁺CD48⁻CD34⁻CD150⁺. For transplantation experiments, LT-HSCs were sorted with FACS sorter (SONY, SH800), mixed with 3×10^5 Sca-1-depleted helper cells and transplanted into lethally irradiated (9.5 Gy) recipient mice. For the HSPCs sorting for 10X Genomics single-cell library preparation, we first transplanted old CD150^{low} or CD150^{high} HSCs (CD45.2) into irradiated young recipient (CD45.1) mice. Fourteen days later, bone marrow cells were collected, and the lineage-positive cells were removed using selection beads. The remaining cells were then stained with antibodies targeting CD45.1, CD45.2, Sca-1, and c-Kit, and CD45.2 LSK cells were sorted for 10X Genomics library preparation.

Cell cycle and DNA damage marker γ H2AX analysis of HSCs with FACS

The analysis of cell cycle status of HSCs was performed as previously described.⁵¹ Briefly, bone marrow cells were prepared, enriched, and stained with HSC marker antibodies as mentioned before. Then the enriched bone marrow cells were fixed and permeabilized with BD Intra Kit (#641776). After washing, fixed HSCs were stained with monoclonal antibody against mouse Ki67 (eBioscience, #11-5698-80) and Hoechst33342 (Thermo Scientific, #R37165) or with antibody against DNA damage marker γ H2AX (Cell Signaling Technology, #97195). The stained cells were analyzed with FACS after washing.

Bulk RNA-seq library preparation

Bulk RNA-seq library was constructed based on Smart-seq2.⁸² SMART-Seq v4 Ultra Low Input RNA Kit for Sequencing (Takara catalog, #634890) was used and experiments were performed according to the manufacturer's instructions.

scRNA-seq library preparation

scRNA-seq library was prepared with Chromium Next GEM Single Cell 3' Reagent Kits V3.1 (Dual Index) from 10X Genomics according to the manufacturer's instruction and previously described method.⁵³

PB analysis via FACS

For PB analysis, up to 30 μ L vein blood was collected from retro orbital sinus or tail tips into EDTA-coated tubes. Red blood cells were first removed by red blood cell lysis buffer (ebioscience, catalog #00-4333-57). The remaining white blood cells were stained with mixed monoclonal conjugated antibodies (CD45.1, CD45.2, CD3, B220, Gr-1 and CD11b). After incubation in 4 °C and darkness for 30 min, PB was analyzed by FACS (BD FICR canto-II).

HSC culture in vitro

Sorted LT-HSCs were cultured in StemSpan™ SFEM II (STEM CELL, catalog #09605) with 10 ng/mL SCF (PeproTech, catalog #AF-250-03), 100 ng/mL TPO (PeproTech, catalog #315-14), 25 ng/mL Flt3L (PeproTech, catalog #250-31 L) and 25 ng/mL IL3 (PeproTech, catalog # 213-13). Six days after culture, the number of HSCs were quantified by FACS (BD FICR canto-II). For the proliferation curve, single HSC was sorted and cultured. The cell number was counted and recorded every day.

Complete blood counting analysis of recipient mice

For whole mouse blood analysis, 75 μ L vein blood was collected from retro orbital sinus and mixed with 225 μ L 5 mM EDTA. Freshly collected whole blood was analyzed by Hematology system (ADVIA 120) within 2 h after collection.

Naïve T, Tcm and Tem analysis

We analyzed the ratio of Naïve T cells, Tcm and Tem based on a previous report.⁸⁴ Briefly, PB was collected and red blood cells were removed by red blood cell lysis buffer (ebioscience, catalog #00-4333-57). The remaining cells were stained with antibodies against CD45.1, CD45.2, CD4, CD8, CD44 and CD62L. T cell subtypes were defined as follows: naïve (CD62L^{high}CD44^{low}), Tcm (CD62L^{high}CD44^{high}) and Tem (CD62L^{low}CD44^{high}).

Physical function tests of mouse

Grip strength was tested by placing mice on a grid strength meter (Bioseb, Model GT3) so only their forepaws grasped the grid. Their tails were pulled

three times, then they rested for at least 1 min. We averaged the top three maximum grip strengths and normalized for body weight.

Beam balance test was performed with homemade equipment: a 1-meter smooth wood strip elevated 50 cm. Mice were trained on a thicker pole (28 mm diameter) until they could cross without dropping. The next day, they were tested three times on the thicker or thinner pole (17 mm diameter). Latent time to cross was recorded.

For pole test, mice were placed at the top of a 50-cm grooved metal pole with a diameter of 1 cm with the mice head pointing down. The time from initial placement on the top of the pole to the time the mouse reached the base of the pole (forelimb contact with platform) was recorded with a stopwatch. Following a 30-min rest in their home cage, the trial was repeated another 2 times. The average time is calculated as the latent time to go down for each mouse.

The rotarod test assessed motor coordination and balance. Mice were placed on an accelerating Rotarod (Ugo Basile Apparatus) starting at 4 rpm. On day one, mice were trained at 4 rpm for 5 min, repeated twice. On test day, the rod accelerated from 4 rpm to 40 rpm over 5 min. Time and speed were recorded when mice dropped or after two passive rotations. Each mouse performed three tests over two days. Results were averaged over these tests.

For the wire hanging test, mice were placed on a metal grid with 1 cm mesh, elevated 50 cm above a cushioned surface with ~3-cm bedding. Mice were put on the metal grid, which was slowly inverted so they hung upside down. The time until the mouse fell was recorded. Each mouse was tested three times with 30-min intervals, and results were averaged.

For treadmill fatigue test, the protocol was adapted and modified from a previous publication.⁸⁵ Briefly, mice were acclimated to the treadmill (Columbus Instruments) for 2 days before testing. The fatigue zone was set as one mouse body-length from the shock grid. On day 1, mice explored the treadmill for 5 min with the shock grid off, then ran at 6 m/min for 5 min with the shock grid on (1.5 mA, 3 Hz). Speed increased by 2 m/min every 2 min, stopping when mice ran at 10 m/min for 5 min. On day 2, the same protocol was followed with a top speed of 12 m/min. On the test day, speed increased stepwise up to a maximum of 26 m/min. Fatigue was defined when mice remained in the fatigue zone for over 5 s on three occasions. Latency to fatigue was recorded for analysis.

For the fear conditioning test, we used contextual and cued fear conditioning (CCFC). On day one, mice underwent 2 min of acclimation, followed by a 30-s tone and a 2-s foot shock (0.5 mA), then a 2-min intertrial interval; this sequence was repeated once more. The next day, mice were placed in the same context for 5 min without shock or tone (context test). On day three, mice were assessed in a modified context: 3 min without tone, then 3 min with tone (cued test). Video was captured using Noldus MediaRecorder 4.0, and freezing behavior was analyzed using Noldus EthoVision XT17.

For the Novel Y-Maze test, adapted from a previous study,⁸⁶ mice were pre-acclimated in a separate holding room for 30 min. The procedure included a 3-min habituation phase with one arm blocked, followed by a 3-min test phase, separated by a strict 2-min intertrial interval. Before the test phase, the obstruction was removed, the maze cleaned, and mice were placed back into the start arm for the test trial. Distance and time traveled were recorded and analyzed using Noldus EthoVision XT17.

Open field testing used a transparent enclosure with a base of 27.3 cm \times 27.3 cm and walls 20.3 cm high; the central zone was half of the total area. Mice were acclimated for at least 20 min prior to testing. Each mouse was placed in the center to begin assessment. Movements were tracked for 20 min using a tracking system (Med Associates, ENV-510), with data collected every 5 min. Analysis included total distance moved, average speed, active and inactive periods, and vertical events during the first 10 min.

Reduced-representation bisulfite sequencing (RRBS) library preparation for HSCs

FACS sorted HSCs were lysed at 50 °C for 3 h and 75 °C for 30 min in 5 μ L lysis buffer (20 mM tris-EDTA, 20 mM KCl, 0.3% Triton X-100, and 1 mg/mL protease). The lysed cells were then subject to MspI digestion at 37 °C for 3 h and 80 °C for 20 min. Following enzymatic digestion, end-repair mix (1 μ L Klenow frag exo (5 U/ μ L), 0.2 μ L of 10 \times TangoBuf, and 0.8 μ L of dNTP mix) was added and incubated at 37 °C for 40 min and 75 °C for 15 min. For adaptor ligation, the reaction was incubated at 16 °C for 30 min, 4 °C overnight, and 65 °C for 20 min after adding the ligation mix (2.25 μ L H₂O, 1 μ L T4 ligase (30 U/ μ L), 0.5 μ L 100 mM ATP, and 0.75 μ M methylated adaptor). Bisulfite conversion reaction was then performed with the EpiTect Bisulfite Kit (Qiagen, catalog #59104) following the manufacturer's instructions. Adapter-tagged BS-

DNA was then amplified by 16 cycles using Kapa HiFi Uracil+ ReadyMix (Kapa Biosystems, catalog #KK2801) with NEBNext Multiplex Oligos for Illumina (New England Biolabs, catalog # E7500L).

ATAC-seq library construction

About 500–1000 cells were sorted by FACS to 10 μ L tagmentation buffer (33 mM Tris-Acetate, 66 mM K-Acetate, 10 mM Mg-Acetate, 16% Dimethylformamide, and 0.02% Digitonin). Then, 0.5 μ L Tn5-Adapter complex (Diagenode) was added and incubated at 37°C for 30 min. The tagmentation reaction was stopped by adding 10 μ L stop buffer (100 mM Tris-HCl, pH 8.0, 100 mM NaCl, 0.4% SDS, 40 μ g/mL Proteinase K) and the samples were incubated at 55°C overnight to release the fragments. SDS was then quenched by adding 5 μ L 25% Tween-20 and incubated on ice for 10 min. Next, 25 μ L samples were mixed with 30 μ L High-Fidelity PCR Master Mix (NEB), 2.5 μ L P5 primer (10 μ M) and 2.5 μ L P7 primer (10 μ M) for PCR amplification. The PCR products were then purified before sequencing.

RNA-seq data analysis

For bulk RNA-seq datasets, adaptor of all sequenced reads was first trimmed by Trim Galore with parameter “-illumina -paired”. Then the filtered reads were aligned to the mm10 reference genome by Hisat2 (Version 2.0.0-b)⁸⁷ with parameters “--no-mixed --no-discordant --dta-cufflinks --no-unal”. The aligned SAM files were then converted to BAM files with Samtools (Version 1.14)⁸⁸ for further analysis. Next, HTSeq-count (V0.12.4)⁸⁹ was used to calculate the count of reads for each gene, with the main parameters set as: “-f bam -s no -r pos”. The reference genome was downloaded from the UCSC Table Browser. To quantify gene expression, the read count for each gene was normalized using DESeq2 (V1.22.2).⁹⁰ The differentially expressed genes from each group were filtered with following criteria: adjusted *P* value < 0.05 and fold-change > 2 or < 0.5.

ATAC-seq analysis

For ATAC-seq datasets, sequencing adaptors and low-quality reads were removed by Trim Galore with parameters: -q 20 --length 30 --paired. The clean reads were mapped to mouse reference genome (mm10) by bowtie2 (Version 2.5.1) with parameter: “-N 1 -L 25 -X 2000 -no-discordant”. After converting aligned SAM to BAM files using Samtools (Version 1.13), Picard (Version 2.26.4) was used for removing PCR duplications. Next, read counts were normalized by Reads Per Kilobase per Million mapped reads (RPKM) and converted to bigwig via bamCoverage (Version 3.5.1). The peaks were called by MACS2 (Version 2.2.7.1)⁹¹ with parameter “-t file -f BED -g mm -outdir OUTPUT -n NAME --nomodel --nolambda”. The peaks that overlap in more than 60% of the replicate samples in each group were kept for feature counts and subsequent analysis using DiffBind (V3.0.15).⁹² Peaks that differed significantly between groups were identified using DESeq2 with the following criteria: *P* value < 0.05 and fold-change > 1.5 or < 0.67. DeepTools (Version 3.5.1)⁹³ was used to visualize the read coverages at peak regions. Motif calling and peak annotation was performed using HOMER (V4.10) with all identified peaks as background. The genes within 5 kb of analyzed peaks were regarded as peak-related genes.

scRNA-seq data analysis

Paired reads from scRNA-seq were first aligned to mm10 reference genome with Cellranger --count (Version 3.0.2) from 10X Genomics. Transcriptome annotation composed of protein-coding genes was downloaded and processed from Ensemble (released-102). To eliminate low-quality single cells, we filtered out single cells with feature numbers below 800 for freshly isolated HSCs (Fig. 2) and below 2000 for short-term transplanted HSCs (Fig. 4). Additionally, cells with mitochondrial transcripts accounting for more than 5 percent were also removed. Then, the remaining single cells were processed and analyzed with Seurat (V4.0.2).⁹⁴ The young and old single cell data are first merged and then normalized and scaled. Two thousand variable feature genes were identified and used for UMAP presentation. The pseudo time analysis was performed using Monocle (Version 2.22.0).⁹⁵ The ordering genes are the marker genes of different cell types from previous report.^{50,61} The single cell GSEA analysis was performed using ClusterProfiler (Version 4.2.2).⁹⁶

Epigenetic age calculation

Paired sequencing files from RRBS were first merged and processed as a single file. Adaptors of all sequenced reads were trimmed by Trim Galore

with parameters “-illumina”. Adaptor trimmed reads were mapped using Bismark (V0.20.0)⁹⁷ using parameters “--fastq -L 30 -N 1 --non_directional”. Methylated CpGs were interpreted by bismark_methylation_extractor with parameter “-s --no_overlap --report -bedGraph”. For base resolution 5mC level calculation, a cutoff of minimal 3 \times coverage was required for each CpG site. Epigenetic age was calculated based on the identified sites and parameters from a previous study.⁹⁸

DATA AVAILABILITY

The dataset generated in this study is summarized in Supplementary information, Table S7. All data have been deposited to GEO with the accession number GSE233879.

REFERENCES

- Brunet, A., Goodell, M. A. & Rando, T. A. Ageing and rejuvenation of tissue stem cells and their niches. *Nat. Rev. Mol. Cell Biol.* **24**, 45–62 (2023).
- Rando, T. A. & Jones, D. L. Regeneration, rejuvenation, and replacement: Turning back the clock on tissue aging. *Cold Spring Harb. Perspect. Biol.* **13**, a040907 (2021).
- López-Otin, C., Blasco, M. A., Partridge, L., Serrano, M. & Kroemer, G. Hallmarks of aging: An expanding universe. *Cell* **186**, 243–278 (2023).
- Kennedy, B. K. et al. Geroscience: linking aging to chronic disease. *Cell* **159**, 709–713 (2014).
- Castellano, J. M., Kirby, E. D. & Wyss-Coray, T. Blood-borne revitalization of the aged brain. *JAMA Neurol.* **72**, 1191–1194 (2015).
- Villeda, S. A. et al. Young blood reverses age-related impairments in cognitive function and synaptic plasticity in mice. *Nat. Med.* **20**, 659–663 (2014).
- Conboy, I. M. et al. Rejuvenation of aged progenitor cells by exposure to a young systemic environment. *Nature* **433**, 760–764 (2005).
- Conese, M., Carbone, A., Beccia, E. & Angiolillo, A. The fountain of youth: A tale of parabiosis, stem cells, and rejuvenation. *Open Med.* **12**, 376–383 (2017).
- Katsimpardi, L. et al. Vascular and neurogenic rejuvenation of the aging mouse brain by young systemic factors. *Science* **344**, 630–634 (2014).
- Sinha, M. et al. Restoring systemic GDF11 levels reverses age-related dysfunction in mouse skeletal muscle. *Science* **344**, 649–652 (2014).
- Jaiswal, S. et al. Age-related clonal hematopoiesis associated with adverse outcomes. *N. Engl. J. Med.* **371**, 2488–2498 (2014).
- Rossi, D. J. et al. Cell intrinsic alterations underlie hematopoietic stem cell aging. *Proc. Natl. Acad. Sci. USA* **102**, 9194–9199 (2005).
- Sudo, K., Ema, H., Morita, Y. & Nakauchi, H. Age-associated characteristics of murine hematopoietic stem cells. *J. Exp. Med.* **192**, 1273–1280 (2000).
- Verovskaya, E. et al. Heterogeneity of young and aged murine hematopoietic stem cells revealed by quantitative clonal analysis using cellular barcoding. *Blood* **122**, 523–532 (2013).
- Jaiswal, S. & Ebert, B. L. Clonal hematopoiesis in human aging and disease. *Science* **366**, eaan4673 (2019).
- Das, M. M. et al. Young bone marrow transplantation preserves learning and memory in old mice. *Commun. Biol.* **2**, 73 (2019).
- Guderyon, M. J. et al. Mobilization-based transplantation of young-donor hematopoietic stem cells extends lifespan in mice. *Aging Cell* **19**, e13110 (2020).
- Li, J. et al. Long-term repopulation of aged bone marrow stem cells using young Sca-1 cells promotes aged heart rejuvenation. *Aging Cell* **18**, e13026 (2019).
- Guest, I., Ilic, Z., Scoble, H. & Sell, S. Survival of irradiated recipient mice after transplantation of bone marrow from young, old and “early aging” mice. *Aging (Albany NY)* **7**, 1212–1223 (2015).
- Leins, H. et al. Aged murine hematopoietic stem cells drive aging-associated immune remodeling. *Blood* **132**, 565–576 (2018).
- Moehrl, B. M. & Geiger, H. Aging of hematopoietic stem cells: DNA damage and mutations? *Exp. Hematol.* **44**, 895–901 (2016).
- Mansell, E. et al. Mitochondrial potentiation ameliorates age-related heterogeneity in hematopoietic stem cell function. *Cell Stem Cell* **28**, 241–256.e246 (2021).
- Florian, M. C. et al. Cdc42 activity regulates hematopoietic stem cell aging and rejuvenation. *Cell Stem Cell* **10**, 520–530 (2012).
- Florian, M. C. et al. Aging alters the epigenetic asymmetry of HSC division. *PLoS Biol.* **16**, e2003389 (2018).
- Mejia-Ramirez, E. & Florian, M. C. Understanding intrinsic hematopoietic stem cell aging. *Haematologica* **105**, 22–37 (2020).
- Sun, D. et al. Epigenomic profiling of young and aged HSCs reveals concerted changes during aging that reinforce self-renewal. *Cell Stem Cell* **14**, 673–688 (2014).
- Beerman, I., Seita, J., Inlay, M. A., Weissman, I. L. & Rossi, D. J. Quiescent hematopoietic stem cells accumulate DNA damage during aging that is repaired upon entry into cell cycle. *Cell Stem Cell* **15**, 37–50 (2014).

28. Chen, X. et al. Bone marrow myeloid cells regulate myeloid-biased hematopoietic stem cells via a histamine-dependent feedback loop. *Cell Stem Cell* **21**, 747–760.e7 (2017).
29. Pinho, S. et al. Lineage-biased hematopoietic stem cells are regulated by distinct niches. *Dev. Cell* **44**, 634–641.e4 (2018).
30. Morita, Y., Ema, H. & Nakauchi, H. Heterogeneity and hierarchy within the most primitive hematopoietic stem cell compartment. *J. Exp. Med.* **207**, 1173–1182 (2010).
31. Kim, K. M. et al. Taz protects hematopoietic stem cells from an aging-dependent decrease in PU.1 activity. *Nat. Commun.* **13**, 5187 (2022).
32. Beerman, I. et al. Functionally distinct hematopoietic stem cells modulate hematopoietic lineage potential during aging by a mechanism of clonal expansion. *Proc. Natl. Acad. Sci. USA* **107**, 5465–5470 (2010).
33. Gulati, G. S. et al. Neogenin-1 distinguishes between myeloid-biased and balanced Hoxb5 (+) mouse long-term hematopoietic stem cells. *Proc. Natl. Acad. Sci. USA* **116**, 25115–25125 (2019).
34. Montecino-Rodriguez, E. et al. Lymphoid-biased hematopoietic stem cells are maintained with age and efficiently generate lymphoid progeny. *Stem Cell Rep.* **12**, 584–596 (2019).
35. Liang, R. et al. Restraining lysosomal activity preserves hematopoietic stem cell quiescence and potency. *Cell Stem Cell* **26**, 359–376.e7 (2020).
36. Challen, G. A., Boles, N. C., Chambers, S. M. & Goodell, M. A. Distinct hematopoietic stem cell subtypes are differentially regulated by TGF- β 1. *Cell Stem Cell* **6**, 265–278 (2010).
37. Foudi, A. et al. Analysis of histone 2B-GFP retention reveals slowly cycling hematopoietic stem cells. *Nat. Biotechnol.* **27**, 84–90 (2009).
38. Qiu, J., Papatsenko, D., Niu, X., Schaniel, C. & Moore, K. Divisional history and hematopoietic stem cell function during homeostasis. *Stem Cell Rep.* **2**, 473–490 (2014).
39. Bernitz, J. M., Kim, H. S., MacArthur, B., Sieburg, H. & Moore, K. Hematopoietic stem cells count and remember self-renewal divisions. *Cell* **167**, 1296–1309.e10 (2016).
40. Morrison, S. J., Wandycz, A. M., Akashi, K., Globerson, A. & Weissman, I. L. The aging of hematopoietic stem cells. *Nat. Med.* **2**, 1011–1016 (1996).
41. Kuribayashi, W. et al. Limited rejuvenation of aged hematopoietic stem cells in young bone marrow niche. *J. Exp. Med.* **218**, e20192283 (2021).
42. Hao, T. et al. An aging mouse model of human chronic myeloid leukemia. *Oncogene* **40**, 3152–3163 (2021).
43. Cossarizza, A. et al. CD45 isoforms expression on CD4+ and CD8+ T cells throughout life, from newborns to centenarians: implications for T cell memory. *Mech. Ageing Dev.* **86**, 173–195 (1996).
44. van der Geest, K. S. et al. Aging disturbs the balance between effector and regulatory CD4+ T cells. *Exp. Gerontol.* **60**, 190–196 (2014).
45. Horvath, S. & Raj, K. DNA methylation-based biomarkers and the epigenetic clock theory of ageing. *Nat. Rev. Genet.* **19**, 371–384 (2018).
46. Flohr Svendsen, A. et al. A comprehensive transcriptome signature of murine hematopoietic stem cell aging. *Blood* **138**, 439–451 (2021).
47. Booth, L. N. & Brunet, A. The aging epigenome. *Mol. Cell* **62**, 728–744 (2016).
48. Pal, S. & Tyler, J. K. Epigenetics and aging. *Sci. Adv.* **2**, e1600584 (2016).
49. Sen, P., Shah, P. P., Nativio, R. & Berger, S. L. Epigenetic mechanisms of longevity and aging. *Cell* **166**, 822–839 (2016).
50. Itokawa, N. et al. Epigenetic traits inscribed in chromatin accessibility in aged hematopoietic stem cells. *Nat. Commun.* **13**, 2691 (2022).
51. Shcherbina, A. et al. Dissecting murine muscle stem cell aging through regeneration using integrative genomic analysis. *Cell Rep.* **32**, 107964 (2020).
52. Wang, J. et al. ATAC-Seq analysis reveals a widespread decrease of chromatin accessibility in age-related macular degeneration. *Nat. Commun.* **9**, 1364 (2018).
53. Kulkarni, R. & Kale, V. Physiological cues involved in the regulation of adhesion mechanisms in hematopoietic stem cell fate decision. *Front. Cell Dev. Biol.* **8**, 611 (2020).
54. Nakamura-Ishizu, A. & Suda, T. Aging of the hematopoietic stem cells niche. *Int. J. Hematol.* **100**, 317–325 (2014).
55. Patrick, R. et al. The activity of early-life gene regulatory elements is hijacked in aging through pervasive AP-1-linked chromatin opening. *Cell Metab.* **36**, 1858–1881.e1823 (2024).
56. Yu, X., Wang, Y., Song, Y., Gao, X. & Deng, H. AP-1 is a regulatory transcription factor of inflammaging in the murine kidney and liver. *Ageing Cell* **22**, e13858 (2023).
57. Burda, P., Laslo, P. & Stopka, T. The role of PU.1 and GATA-1 transcription factors during normal and leukemogenic hematopoiesis. *Leukemia* **24**, 1249–1257 (2010).
58. Laramée, A. S. et al. Opposing Roles for the Related ETS-Family Transcription Factors Spi-B and Spi-C in Regulating B Cell Differentiation and Function. *Front. Immunol.* **11**, 841 (2020).
59. Beerman, I. Accumulation of DNA damage in the aged hematopoietic stem cell compartment. *Semin. Hematol.* **54**, 12–18 (2017).
60. Li, T., Zhou, Z. W., Ju, Z. & Wang, Z. Q. DNA damage response in hematopoietic stem cell ageing. *Genomics Proteom. Bioinforma.* **14**, 147–154 (2016).
61. Rodriguez-Fraticelli, A. E. et al. Clonal analysis of lineage fate in native haematopoiesis. *Nature* **553**, 212–216 (2018).
62. Sharifi, S., da Costa, H. F. R. & Bierhoff, H. The circuitry between ribosome biogenesis and translation in stem cell function and ageing. *Mech. Ageing Dev.* **189**, 111282 (2020).
63. Signer, R. A., Magee, J. A., Salic, A. & Morrison, S. J. Haematopoietic stem cells require a highly regulated protein synthesis rate. *Nature* **509**, 49–54 (2014).
64. Wang, R. & Amoyel, M. mRNA translation is dynamically regulated to instruct stem cell fate. *Front. Mol. Biosci.* **9**, 863885 (2022).
65. Ergen, A. V. & Goodell, M. A. Mechanisms of hematopoietic stem cell aging. *Exp. Gerontol.* **45**, 286–290 (2010).
66. Sigurdsson, V. & Miharada, K. Regulation of unfolded protein response in hematopoietic stem cells. *Int. J. Hematol.* **107**, 627–633 (2018).
67. Demerdash, Y., Kain, B., Essers, M. A. G. & King, K. Y. Yin and Yang: The dual effects of interferons on hematopoiesis. *Exp. Hematol.* **96**, 1–12 (2021).
68. Ito, K. & Suda, T. Metabolic requirements for the maintenance of self-renewing stem cells. *Nat. Rev. Mol. Cell Biol.* **15**, 243–256 (2014).
69. Chen, C., Liu, Y., Liu, Y. & Zheng, P. mTOR regulation and therapeutic rejuvenation of aging hematopoietic stem cells. *Sci. Signal.* **2**, ra75 (2009).
70. Kiel, M. J. et al. SLAM family receptors distinguish hematopoietic stem and progenitor cells and reveal endothelial niches for stem cells. *Cell* **121**, 1109–1121 (2005).
71. Young, K. et al. Decline in IGF1 in the bone marrow microenvironment initiates hematopoietic stem cell aging. *Cell Stem Cell* **28**, 1473–1482.e7 (2021).
72. Wendorff, A. A. et al. Epigenetic reversal of hematopoietic stem cell aging in Phf6-knockout mice. *Nat. Aging* **2**, 1008–1023 (2022).
73. Ergen, A. V., Boles, N. C. & Goodell, M. A. Rantes/Ccl5 influences hematopoietic stem cell subtypes and causes myeloid skewing. *Blood* **119**, 2500–2509 (2012).
74. Ocampo, A. et al. In vivo amelioration of age-associated hallmarks by partial reprogramming. *Cell* **167**, 1719–1733.e12 (2016).
75. Browder, K. C. et al. In vivo partial reprogramming alters age-associated molecular changes during physiological aging in mice. *Nat. Aging* **2**, 243–253 (2022).
76. Lu, Y. et al. Reprogramming to recover youthful epigenetic information and restore vision. *Nature* **588**, 124–129 (2020).
77. Schroer, A. B. et al. Platelet factors attenuate inflammation and rescue cognition in ageing. *Nature* **620**, 1071–1079 (2023).
78. Smith, S. C. et al. GDF11 does not rescue aging-related pathological hypertrophy. *Circ. Res.* **117**, 926–932 (2015).
79. Egerman, M. A. et al. GDF11 increases with age and inhibits skeletal muscle regeneration. *Cell Metab.* **22**, 164–174 (2015).
80. Ross, J. B. et al. Depleting myeloid-biased haematopoietic stem cells rejuvenates aged immunity. *Nature* **628**, 162–170 (2024).
81. Szade, K., Bukowska-Strakova, K., Zukowska, M., Jozkowicz, A. & Dulak, J. Analysis of cell cycle status of murine hematopoietic stem cells. *Methods Mol. Biol.* **1516**, 91–99 (2016).
82. Picelli, S. et al. Smart-seq2 for sensitive full-length transcriptome profiling in single cells. *Nat. Methods* **10**, 1096–1098 (2013).
83. Chen, R. et al. Decoding molecular and cellular heterogeneity of mouse nucleus accumbens. *Nat. Neurosci.* **24**, 1757–1771 (2021).
84. Pakpour, N., Zaph, C. & Scott, P. The central memory CD4+ T cell population generated during Leishmania major infection requires IL-12 to produce IFN- γ . *J. Immunol.* **180**, 8299–8305 (2008).
85. Dougherty, J. P., Springer, D. A. & Gershengorn, M. C. The treadmill fatigue test: A simple, high-throughput assay of fatigue-like behavior for the mouse. *J. Vis. Exp.* **111**, e54052 (2016).
86. Chen, R. et al. Cell type-specific mechanism of Setd1a heterozygosity in schizophrenia pathogenesis. *Sci. Adv.* **8**, eabm1077 (2022).
87. Kim, D., Langmead, B. & Salzberg, S. L. HISAT: A fast spliced aligner with low memory requirements. *Nat. Methods* **12**, 357–360 (2015).
88. Danecek, P. et al. Twelve years of SAMtools and BCFtools. *Gigascience* **10**, giab008 (2021).
89. Anders, S., Pyl, P. T. & Huber, W. HTSeq—a Python framework to work with high-throughput sequencing data. *Bioinformatics* **31**, 166–169 (2015).
90. Love, M. I., Huber, W. & Anders, S. Moderated estimation of fold change and dispersion for RNA-seq data with DESeq2. *Genome Biol.* **15**, 550 (2014).
91. Zhang, Y. et al. Model-based analysis of ChIP-Seq (MACS). *Genome Biol.* **9**, R137 (2008).
92. Ross-Innes, C. S. et al. Differential oestrogen receptor binding is associated with clinical outcome in breast cancer. *Nature* **481**, 389–393 (2012).
93. Ramirez, F. et al. deepTools2: a next generation web server for deep-sequencing data analysis. *Nucleic Acids Res.* **44**, W160–W165 (2016).
94. Hao, Y. et al. Integrated analysis of multimodal single-cell data. *Cell* **184**, 3573–3587.e29 (2021).

95. Trapnell, C. et al. The dynamics and regulators of cell fate decisions are revealed by pseudotemporal ordering of single cells. *Nat. Biotechnol.* **32**, 381–386 (2014).
96. Yu, G., Wang, L. G., Han, Y. & He, Q. Y. clusterProfiler: An R package for comparing biological themes among gene clusters. *Omic* **16**, 284–287 (2012).
97. Krueger, F. & Andrews, S. R. Bismark: A flexible aligner and methylation caller for Bisulfite-Seq applications. *Bioinformatics* **27**, 1571–1572 (2011).
98. Meer, M. V., Podolskiy, D. I., Tyshkovskiy, A. & Gladyshev, V. N. A whole lifespan mouse multi-tissue DNA methylation clock. *Elife* **7**, e40675 (2018).

ACKNOWLEDGEMENTS

We thank Jiayi Li for her assistance in some experiments. We thank the support of Mouse Behavior Core of Harvard Medical School and its director Dr. Barbara Caldarone. This project was supported by the Milky Way Research Foundation and the Howard Hughes Medical Institute (HHMI). Y.Z. is an investigator of the HHMI. This article is subject to HHMI's Open Access to Publications policy. HHMI lab heads have previously granted a nonexclusive CC BY 4.0 license to the public and a sublicensable license to HHMI in their research articles. Pursuant to those licenses, the author-accepted manuscript of this article can be made freely available under a CC BY 4.0 license immediately upon publication.

AUTHOR CONTRIBUTIONS

Y.Z. conceived and supervised the project; Y.W., W.Z. and Y.Z. designed the experiments; Y.W. performed the cell sorting, transplantation, FACS analysis, and physical function tests with help from H.Q.T.V.; W.Z. and Y.W. performed the library preparation for bulk RNA-seq, scRNA-seq, RRBS and ATAC-seq; Y.W., W.Z. and C.Z. analyzed the scRNA-seq data; Y.W. and W.Z. analyzed the bulk RNA-seq and RRBS data; Y.W. and C.Z. analyzed the ATAC-seq data; T.S. helped with the complete blood counting analysis; Y.W., W.Z. and Y.Z. interpreted the data and wrote the manuscript with feedback from all authors.

COMPETING INTERESTS

The authors declare the following competing financial interests: Y.Z. and Y.W. are the inventors of a patent related to the work presented in this manuscript. The patent

number is 63472759 and the title is: "Compositions and Methods for Assessing, Treating, or Reducing Aging-Related Functional Decline", which was filed on June 13, 2023.

ADDITIONAL INFORMATION

Supplementary information The online version contains supplementary material available at <https://doi.org/10.1038/s41422-024-01057-5>.

Correspondence and requests for materials should be addressed to Yi Zhang.

Reprints and permission information is available at <http://www.nature.com/reprints>



Open Access This article is licensed under a Creative Commons Attribution 4.0 International License, which permits use, sharing, adaptation, distribution and reproduction in any medium or format, as long as you give appropriate credit to the original author(s) and the source, provide a link to the Creative Commons licence, and indicate if changes were made. The images or other third party material in this article are included in the article's Creative Commons licence, unless indicated otherwise in a credit line to the material. If material is not included in the article's Creative Commons licence and your intended use is not permitted by statutory regulation or exceeds the permitted use, you will need to obtain permission directly from the copyright holder. To view a copy of this licence, visit <http://creativecommons.org/licenses/by/4.0/>.

© The Author(s) 2024